Constant In-Band Group-Delay Acoustic-Wave-Lumped-Element-Resonator-Based Bandpass Filters and Diplexers

Dimitra Psychogiou, *Member, IEEE*, Roberto Gómez-García, *Senior Member, IEEE*, and Dimitrios Peroulis, *Fellow, IEEE*

Abstract—The RF design of acoustic-wave-resonator-based bandpass filters (BPFs) with constant in-band group delay (τ_g) and analog transfer-function reconfigurability is presented. The proposed filter concept is based on N identical acoustic-wavelumped-element resonators (AWLRs) that are electromagnetically coupled through impedance inverters and result in quasi-elliptictype transfer functions shaped by N poles and 2N transmission zeros (TZs). Unlike conventional ladder- or lattice-type acousticwave-resonator filter configurations, they facilitate: i) flat in-band τ_g that does not depend on the electromechanical coupling coefficient (k_t^2) of its constituent acoustic-wave resonators and does not require the incorporation of lossy elements, ii) passbands with fractional bandwidths (FBWs) that can exceed k_t^2 , and iii) continuous analog-type FBW tuning. The operating principles of the devised concept are presented through two different filter architectures that respectively present advantages in terms of size and FBW tuning, and are subsequently extended to the design of RF diplexers. They are experimentally verified through the following prototypes: i) a three-pole/six-TZ BPF that is centered at 418 MHz and exhibits bandwidth (BW) of 0.3 MHz, minimum in-band insertion loss (IL) of 2.1 dB (i.e., effective quality factor Q_{eff} of 9,000), and in-band τ_g between 1.78 \pm 0.02 μ s, ii) a twopole/four-TZ BPF with 2.4:1 BW tuning ratio, flat τ_g , and Q_{eff} 9,000, and iii) a flat- τ_g diplexer with two transmission bands centered at 418 MHz and 433.9 MHz.

Index Terms—Acoustic-wave (AW) filter, bandpass filter (BPF), constant group delay, flat group delay, RF/microwave filter, surface-acoustic-wave (SAW) resonator.

I. INTRODUCTION

THE unprecedented growth of wireless communication systems and, in particular, the ones operating at the UHF band (300 MHz to 3,000 MHz) are increasingly calling for new developments in the physical layer [1]. These include highly-versatile RF front-end chains able to support multiple operational bands, standards, and waveforms without sacrificing power efficiency and size [2]. RF filtering units shaped by acoustic-wave resonators, such as those based on surface-acoustic-wave (SAW) and bulk-acoustic-wave (BAW)

Manuscript received June 30, 2017; revised on September 20, 2017, accepted January, 9, 2018. This work has been partially supported by the National Science Foundation, award number 1731956.

D. Psychogiou is with the Department of Electrical, Computer and Energy Engineering, University of Colorado Boulder, Boulder, CO 80309, USA (e-mail: dimitra.psychogiou@colorado.edu).

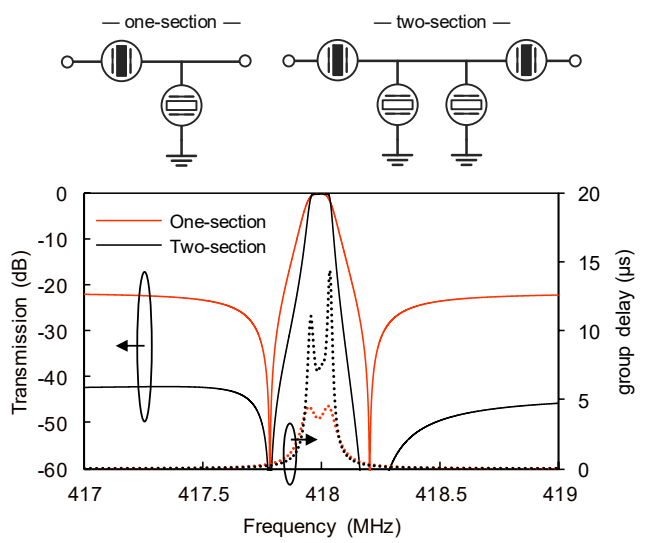


Fig. 1. Frequency response of conventionally-designed ladder-type acoustic-wave-resonator-based BPFs in terms of power transmission response and τ_g . For both BPF designs, lossless one-port-type AWRs with k_r^2 =0.1%, series resonant frequency f_S = 418 MHz for the series acoustic-wave resonator, and series resonant frequency f_S = 417.78 MHz for the parallel acoustic-wave resonator are employed.

resonators, have become the key pre-select filtering technology of wireless transceivers due to their unique advantages in terms of: i) quality factor (Q)—typically of the order of 1,000—, ii) small form factor—1 mm³ to 4 mm³ per resonator for packaged commercially-available SAWs—, and iii) compatibility with low-cost manufacturing and microfabrication [3]-[8]. However, when used in ladder- or lattice-type configurations, their RF performance is limited by narrow fractional bandwidth (FBW)—restricted by the electromechanical coupling coefficient (k_t^2) of its constituent acoustic-wave resonators and is typically between $0.4k_t^2$ and $0.8k_t^2$ —[6], the presence of spurious modes both below and above the passband [7]-[8], and large in-band group-delay (τ_g) variation as shown in the examples in Figs. 1 and 2.

Research efforts in the past decade [3]-[11] have been primarily focusing on: i) enhancing FBW either through the use

R. Gómez-García is with the Department of Signal Theory and Communications, University of Alcalá, Alcalá de Henares, 28871 Madrid, Spain (e-mail: roberto.gomez.garcia@ieee.org).

D. Peroulis is with the School of Electrical and Computer Engineering, Birck Nanotechnology Center, Purdue University, West Lafayette, IN 47907, USA (e-mail: dperouli@purdue.edu).

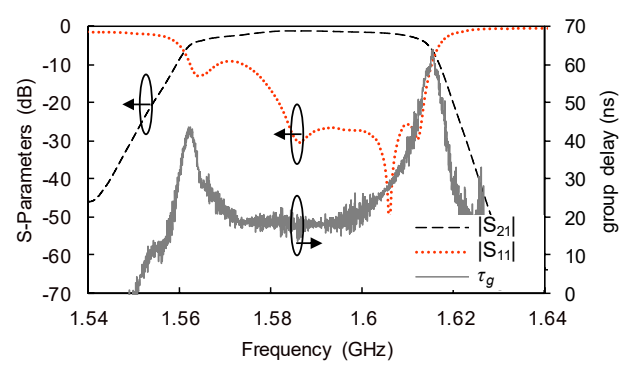


Fig. 2. RF-measured S-parameters and τ_g of a commercially-available SAW-based BPF: Abracon AFS14A35-1591.5-T3 filter.

of dissimilar—i,e., with different resonant frequency and k_t^2 acoustic-wave resonators, or by creating high- k_t^2 materials and, more recently, by co-integrating acoustic-wave-lumpedelement resonators (AWLRs) with electromagnetic (EM) coupling elements [9]-[11], and on ii) suppressing spurious resonances at the expense of higher in-band insertion loss and narrower FBW [2]-[4]. However, none of the aforementioned techniques has considered the in-band τ_g that varies to a large extend. This RF performance limitation is illustrated in Fig. 1, in which the simulated responses of two ladder-type filters that respectively comprise one and two sections—designed using the methodology in [12]—are plotted. It can be seen that the in-band τ_g variation worsens at the edges of the passband and increases as the number of the filter sections gets higher, which may severely distort the RF signals that are transmitted within the filter's passband. The same effect can be also anticipated in Fig. 2 for an off-the-shelf commercially-available SAW-based filter.

To the best of the authors' knowledge, the design of acousticwave-resonator-based BPFs with constant/flat τ_g has not been adequately addressed in the open technical literature. It is mostly limited to two different approaches that either reconfigure the shape of the acoustic-wave resonator's transducers or combine dissimilar acoustic-wave resonators with lossy elements [13]-[15]. However, despite the observed improvement in the in-band τ_g variation, they come at the expense of higher in-band insertion loss (IL: 5.2 dB to 25.5 dB) and increased fabrication/assembly sensitivity due to the use of dissimilar resonators. A summary of these techniques includes the filter architectures in [13]-[15]. In particular, the filter in [13] makes use of slanted interdigital transducers that result in a fairly-constant τ_g (695 ± 10 ns) but with prohibitive levels of in-band IL of around 25.5 dB. In an alternative configuration, resonant single-phase transducers are utilized [14]. They result in a filter passband centered at 512 MHz with τ_g of 562.5 \pm 37.5 ns and high minimum IL of 5.2 dB. Similar RF performance is obtained in [15], in which τ_g flattening is achieved by lowering the Q of the acoustic-wave resonators to 200, which produces increased levels of in-band IL.

Taking into consideration the aforementioned technological limitations, this paper focuses on a simple RF design methodology that, for the first time, addresses the design of quasi-elliptic-type passbands with constant in-band τ_g . The proposed approach is based on N electromagnetically-coupled AWLRs—each of them contributing to the overall transfer

function with one pole and two transmission zeros (TZs). In relation to state-of-the-art acoustic-wave-resonator-based ladder- or lattice-type filters, the devised AWLR-based BPFs exhibit the following unique RF performance characteristics: i) constant in-band τ_g that neither depends on k_t^2 nor requires lowering the Q of its constituent acoustic-wave resonators, ii) FBWs that do not depend on k_t^2 and can be even made wider, iii) continuous and analog FBW tuning whilst preserving the τ_g flatness, and iv) realization with identical acoustic-wave resonators. Preliminary results on this concept were demonstrated by the authors in [16] for the case of a threepole/six-TZ quasi-elliptic-type AWLR-based BPF. In this paper, we extend this concept to two alternative filter topologies, namely Topologies A and B as shown in Fig. 3, for which we provide an in-depth RF design analysis followed by various circuit-level examples. In particular, we address various RF design aspects including narrow and broad FBW realizations and in-band flat τ_g design in the presence of spurious modes. More importantly, we focus on FBW tunability while keeping the in-band τ_g constant and we extend the

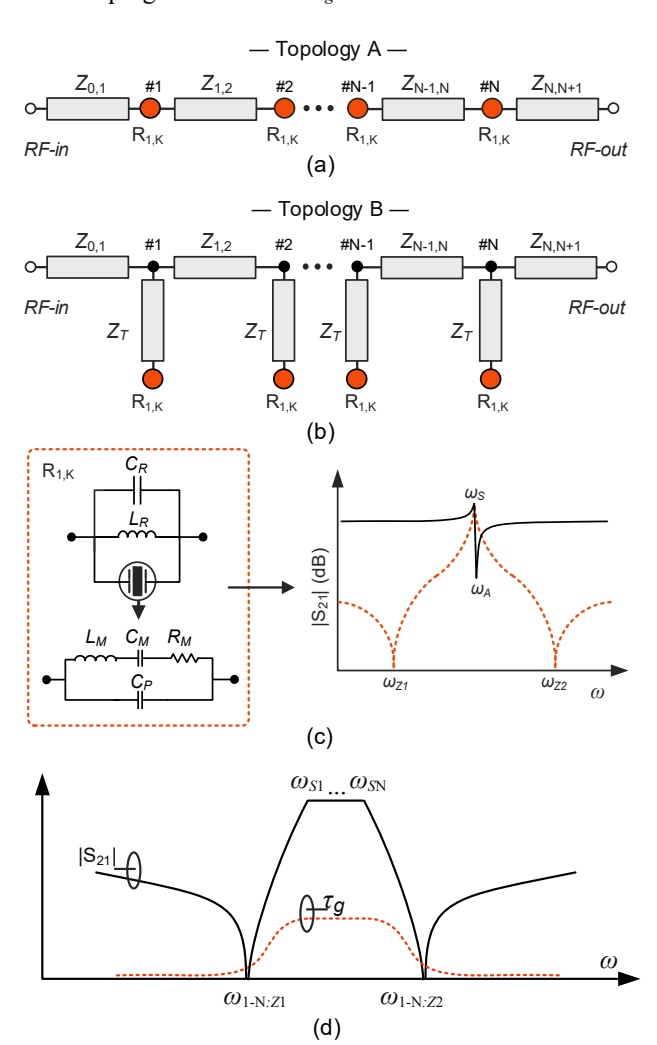


Fig. 3. AWLR-based BPF concept with flat in-band τ_g and quasi-elliptic-type response shaped by N AWLRs that contribute to N poles and 2N TZs. (a) Block diagram of Topology A. (b) Block diagram of Topology B. (c) Circuit schematic and example power transmission response of the AWLR and the one-port-type acoustic-wave resonator. (d) Conceptual power transmission and τ_g responses of Topologies A and B.

proposed design methodology to the realization of constant inband τ_g diplexers. Lastly, we demonstrate two new experimental prototypes using commercially-available SAW resonators, namely a two-pole/four-TZ BPF with continuouslytunable FBW and a diplexer that is shaped by two twopole/four-TZ BPFs centered at 418 MHz and 433.9 MHz.

The content of this work is organized as follows. In Section II, the proposed AWLR-based filter design concept and its relevant RF design principles are presented. In Section III, we focus on the experimental validation of the aforementioned operational principles through the EM design and experimental testing of three proof-of-concept prototypes that exhibit flat inband τ_g and FBW tuning. Lastly, the most relevant contributions of this work are discussed in Section IV.

II. RF DESIGN FOUNDATIONS

The generalized circuit schematic and conceptual transfer function of two different AWLR-based BPF topologies with constant in-band τ_g , namely Topology A—Fig. 3(a)—and Topology B—Fig. 3(b)—, are illustrated in Fig. 3. Whereas both filter architectures are electrically equivalent for a given transfer function, they show advantages in terms of size and BW tunability, respectively, as it will be further explained at this section. We will begin by discussing the basic operating

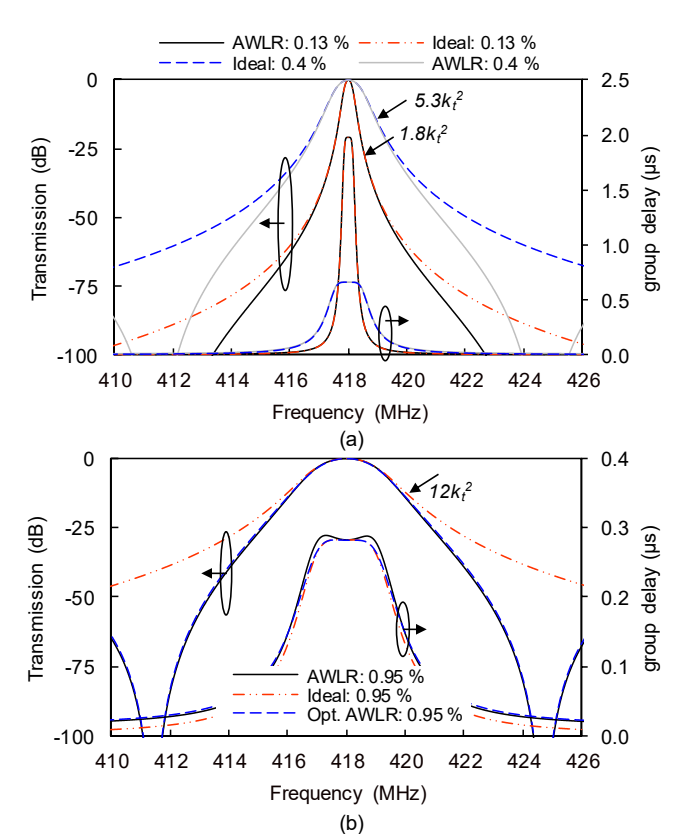


Fig. 4. Power transmission response and τ_g of an ideal Gaussian-type BPF (three poles) and the proposed AWLR-based BPF (three poles and six TZs) with constant in-band τ_g —Topology A—. (a) Narrow-BW states: 0.13% (1.8 k_t^2)— $Z_{0,1}$ = 1.4, $Z_{1,2}$ = 2.9, $Z_{2,3}$ = 7.4, and $Z_{3,4}$ = 3.5— and 0.4% (5.3 k_t^2)— $Z_{0,1}$ = 2.4, $Z_{1,2}$ = 8.7, $Z_{2,3}$ = 2.2, and $Z_{3,4}$ = 6—. (b) Broad-BW states: 0.95% (12 k_t^2)—Ideal: $Z_{0,1}$ = 3.6, $Z_{1,2}$ = 20, $Z_{2,3}$ =52, and $Z_{3,4}$ = 9—. Optimized/finelytuned: $Z_{0,1}$ = 3.6, $Z_{1,2}$ = 20.5, $Z_{2,3}$ =56, and $Z_{3,4}$ = 9.8. The AWLRs consist of acoustic-wave resonators with k_t^2 =0.08%. The indicated impedance values are normalized to the system reference impedance Z_0 .

principles of the proposed concept through Topology A and continue with the design characteristics of Topology B. Furthermore, the RF design of AWLR-based BPFs when spurious modes are present and the design of RF diplexers using AWLRs will be presented.

A. Topology A

The block diagram of Topology A is illustrated in Fig. 3(a). It is based on N identical AWLRs (Nth-order response) that are in-series cascaded with N+1 impedance inverters. Each AWLR one one-port-type acoustic-wave is shaped resonator—motional capacitance C_M , inductance L_M , resistance R_M , and parallel capacitance C_P —that exhibits a series resonant frequency ω_S and anti-resonant frequency ω_A and is cascaded in parallel with an inductor (L_R) and/or a capacitor (C_R) . If the L_R , C_R values are appropriately selected so that they resonate with C_P at ω_S , a single high-Q resonance can be created at ω_S together with two symmetrically-allocated TZs as shown in Fig. 3(c). Further details on the AWLR design can be found in [10]. The devised AWLR-based BPF exhibits a transfer function whose overall shape can be considered quasi-elliptic and comprises N poles and 2N TZs. By appropriately selecting the location of the poles and the TZs through the impedance values of the N+1 inverters, $Z_{0,1}$ - $Z_{N,N+1}$, constant in-band τ_g behavior can be obtained in the passband that in turn resembles a Gaussian-type response.

In order to demonstrate the operational principles of the constant in-band τ_g AWLR-BPF concept, various examples of conventional Gaussian-type BPFs and the proposed AWLR-BPF are shown in Fig. 4 for both narrow (Fig. 4(a)) and broad (Fig. 4(b)) BW states and for an acoustic-wave resonator with C_M = 1.21 fF, L_M =119.6 μ H, C_P =1.2 pF, and k_t ²=0.08%. The illustrated power transmission and τ_g responses have been obtained using circuit-level simulations, in which the component values are specified using (1)-(3) [17, page 58] where g_0 - g_N are the normalized element values of the lowpass Gaussian-type prototype and Z_0 is the system reference impedance.

$$Z_{0,1} = \left(\frac{Z_0 FBW \omega_s L_M}{g_0 g_0}\right)^{0.5} \tag{1}$$

$$Z_{i,i+1} = \frac{FBW \omega_{S} L_{M}}{\left(g_{i}g_{i+1}\right)^{0.5}}$$
 (2)

$$Z_{N,N+1} = \left(\frac{Z_0 FBW \omega_S L_M}{g_N g_{N+1}}\right)^{0.5}$$
(3)

Fig. 4(a) depicts a comparison between the frequency responses of conventional Gaussian-type BPFs and the proposed AWLR BPF for narrow FBW states—obtained using (1)-(3)—. As can be seen, their passband characteristics are in close agreement with each other. On the contrary, when the passband BW becomes wider and its edges get closer to the TZs, small differences in terms of in-band τ_g can be observed. This is illustrated in Fig. 4(b)—red trace versus black trace—. However, they can be readily counteracted by finely adjusting the values— by about 2% to 5% from the ones calculated with

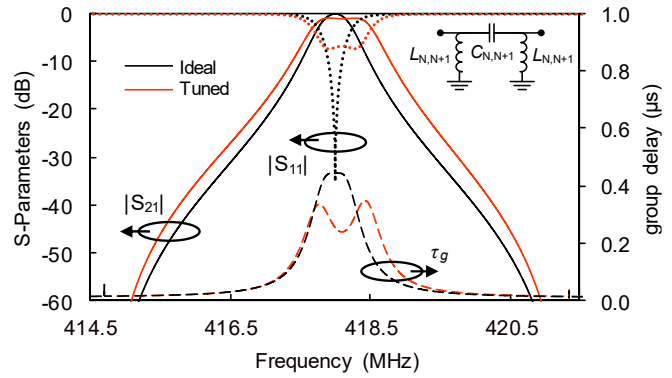


Fig. 5. Synthesized power transmission, reflection, and τ_g responses of a three-pole/six-TZ AWLR-based BPF—Topology A—with constant in-band τ_g and tunable BW. The impedance inverters $Z_{1,2}$, $Z_{2,3}$, $Z_{3,4}$ are realized as 90°-electrically-long-at-418 MHz transmission lines. They are represented by their π -type first-order circuit equivalent ($L_{\rm N,N+1}$, $C_{\rm N,N+1}$) in order to functionalize the narrow-BW state (black trace: $C_{0,1}$ =1.5 pF, $C_{1,2}$ =0.56 pF, $C_{2,3}$ =2.98 pF) and then tuned to a broader-BW state (red trace: $C_{0,1}$ =1.47 pF, $C_{1,2}$ =0.41 pF, $C_{2,3}$ =2.6 pF) by tuning the capacitance of its inverters.

(1)-(3)—of the impedance inverters. As an important advantage to be highlighted in relation to state-of-the-art acoustic-waveresonators filters, the proposed architecture facilitates the realization of FBWs that are not limited by k_t^2 and can be even made wider as shown in the examples in Fig. 4. Note that ladder-/lattice/self-cascaded conventional acoustic-waveresonator filters exhibit FBWs between 0.4 and 0.8 k_t^2 [4]-[8]. Due to the high inductance value of the acoustic-wave resonators (~µH for SAW resonators) for the realization of wide FBW states, high impedance—proportional to L_M —inverters could be required, which may result in unrealizable values. However, this design aspect can be readily counteracted by i) lowering the effective series inductance of the AWLR through the parallel cascade of multiple acoustic-wave resonators or by ii) using Topology B as it will be explained in the next section.

Taking into consideration that transfer-function tunability is of critical importance for multi-standard RF front-ends, we investigated the effect of BW tuning by adjusting the impedance values of the AWLR-BPFs inverters. In a real implementation, this can be achieved by realizing all the inverters by their π -type circuit equivalent (first-order highpass type in this case) and altering its properties through variable capacitors. Such an example is illustrated in Fig. 5 for a threepole/six-TZ AWLR BPF. The black trace represents the filter response when its components are specified using (1)-(3), which is then tuned to exhibit a larger BW state—red trace—by altering the capacitance of its impedance inverters. It can be observed that despite being able to widen the BW, this comes at the expense of increased in-band reflection loss and the appearance of τ_g ripple, making this configuration not suitable for BW tuning under the flat in-band τ_g requisite.

B. Topology B

The generalized circuit schematic of an alternative AWLR-based BPF structure—Topology B—that facilitates the simultaneous realization of BW tuning and constant in-band τ_g is depicted in Fig. 3(b). In relation to Topology A, the AWLRs are in-parallel connected to the source-to-load path—shaped by

the $Z_{0,1}$ - $Z_{N,N+1}$ impedance inverters—through an impedance inverter Z_T . The presence of Z_T also adds flexibility in the selection of the impedance inverters $Z_{0,1}$ - $Z_{N,N+1}$, which now depend on the ratio Z_T^2/L_M as shown in its corresponding design equations (4)-(6). However, the resulting filter architecture is larger than the one of Topology A due to the need for 2N+1 inverters for an N-pole/2N-TZ response.

In order to demonstrate the advantages of this approach, Fig. 6 depicts the power transmission and τ_g responses of a three-pole/six-TZ AWLR-based BPF with tunable BW. Its ideal response (black trace) has been obtained from a filter topology that is designed using (4)-(6).

$$Z_{0,1} = \left(\frac{Z_{0}g_{0}g_{1}Z_{T}^{2}}{FBW\omega_{s}L_{w}}\right)^{0.5}$$
 (4)

$$Z_{i,i+1} = \frac{\left(g_{i}g_{i+1}\right)^{0.5}Z_{T}^{2}}{FBW\omega_{s}L_{M}}$$
 (5)

$$Z_{N,N+1} = \left(\frac{Z_0 g_N g_{N+1} Z_T^2}{FBW \omega_s L_M}\right)^{0.5}$$
 (6)

Note that for wide-FBW states, fine tuning may be required as discussed in the previous section. Furthermore, in relation to the Topology A example in Fig. 5, BW tuning is facilitated by

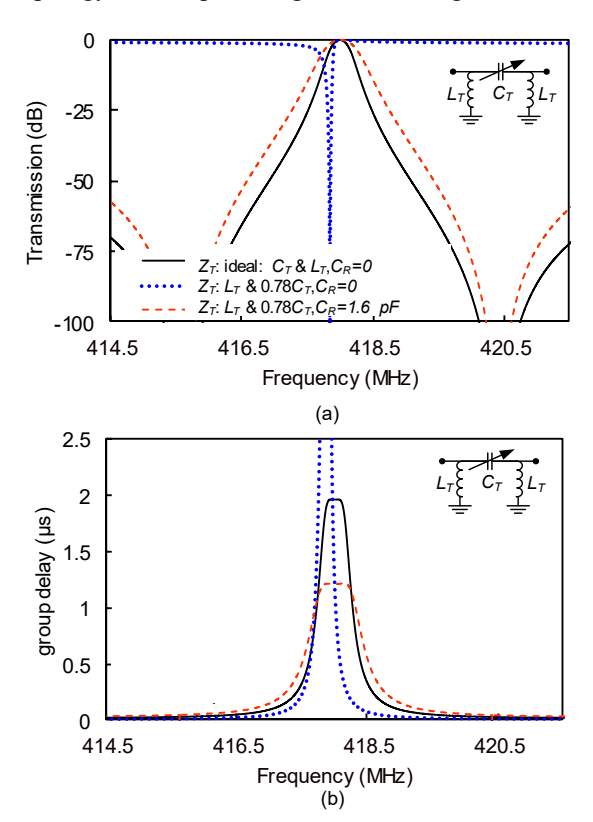


Fig. 6. Power transmission response and τ_g of a three-pole/six-TZ AWLR-based BPF—Topology B—with constant in-band τ_g and tunable BW. The impedance inverters Z_T are realized as 50- Ω 90°-electrically-long-at-418-MHz transmission lines. They are represented by their π -type circuit equivalent (L_T , C_T) in order to functionalize the narrow-BW state (black trace) and then tuned to a broader-BW state (red trace) by decreasing C_T and increasing C_R . (a) Power transmission response. (b) τ_g .

only altering the capacitance of the impedance inverters Z_T — $Z_{0,1}$ - $Z_{N,N+1}$ remain constant—and the AWLRs's capacitance C_R . As can be seen in Fig. 6, wider-BW states can be obtained by lowering C_T . However, it results in an asymmetric transfer function (blue trace) and in the appearance of τ_g ripple. This is attributed to the non-ideal electrical behavior of the impedance inverter (electrical length different from 90° at 418 MHz). These effects can be counteracted by appropriately increasing the AWLR capacitance C_R (in this case from 0 to 1.6 pF) as depicted in the red trace. As such, for the implementation of symmetrical quasi-elliptic-type transfer functions with tunable BW and flat in-band τ_g both C_T and C_R need to be tuned.

C. Comparison of Topology A and B and finite-Q effect

In order to illustrate the RF design trade-offs between Topologies A and B, an example case of two-pole/four-TZ BPFs that have the same FBW is considered and is shown in Fig. 7. The effect of finite Q in the inverters and in the AWLR elements is also analyzed in this figure. It should be highlighted that all inverters have been replaced with their π -type first-order

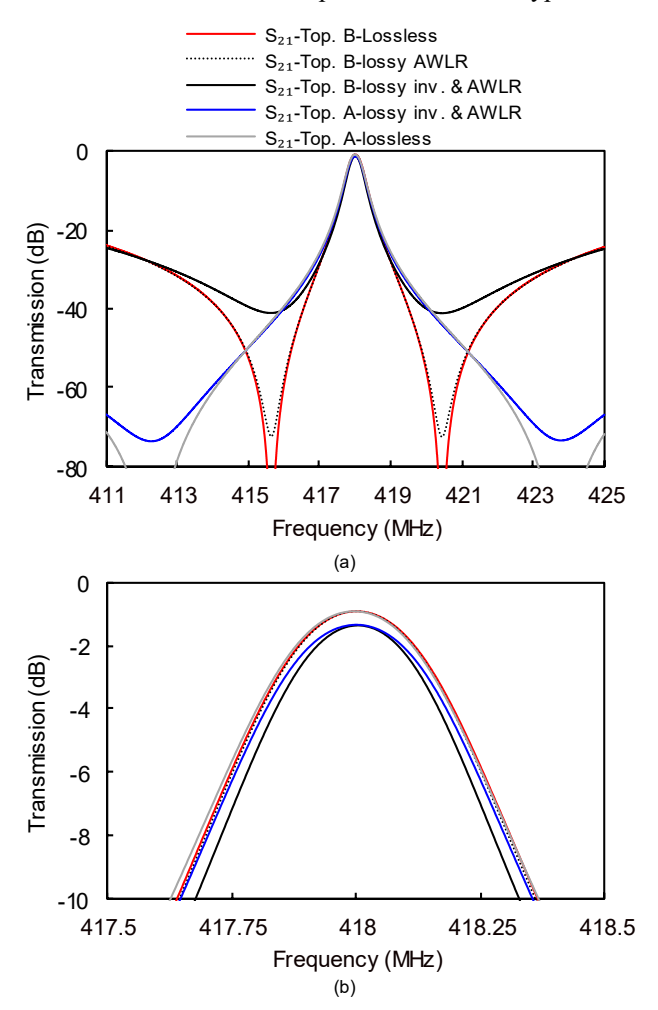


Fig. 7. Simulated power transmission response of two-pole/four-TZ AWLR-based BPFs—Topology A and Topology B—with and without finite Q in the lumped element of the AWLR and the impedance inverters. All impedance inverters have been realized by their first-order π -type circuit equivalent. In all examples the acoustic-wave resonators have been modeled with a Q of 14,100. The examples that consider loss in the lumped elements assume a Q of 100 for the inductors and a Q of 400 for the capacitors.

circuit equivalent and each acoustic-wave resonator is modeled using the circuit equivalent of a commercially-available SAW resonator (ASR418S from Abracon) with f_S =418 MHz, C_M = 1.21 fF, L_M =119.6 μ H, C_P =1.2 pF, and k_t^2 =0.08%. The transfer functions that include loss consider a Q of 100 for the inductors and a O of 400 for the capacitors as typically found in commercially-available SMD elements at this frequency (e.g., inductors from Coilcraft and ceramic capacitors from Johanshon Tech.). As can be seen in Fig. 7, the TZs in Topology B appear closer to the passband than in Topology A. Furthermore, for the same element O, Topology B exhibits lower TZ attenuation than Topology A, however similar inband insertion loss (IL). Note that the amount of added loss in the passband in relation to the lossless scenario is fairly small. For the worst-case-scenario transfer function (Topology B and finite Q is introduced in all filter elements) the in-band IL is only 0.44 dB higher than in the lossless case. It should be highlighted that the resulting in-band IL corresponds to an effective quality factor Q_{eff} of 10,600, which is comparable to the Q of the acoustic-wave-resonator (14,100 in this case). This proves the suitability of the devised AWLR-based BPF concept for the realization of low-loss and highly-selective RF filters.

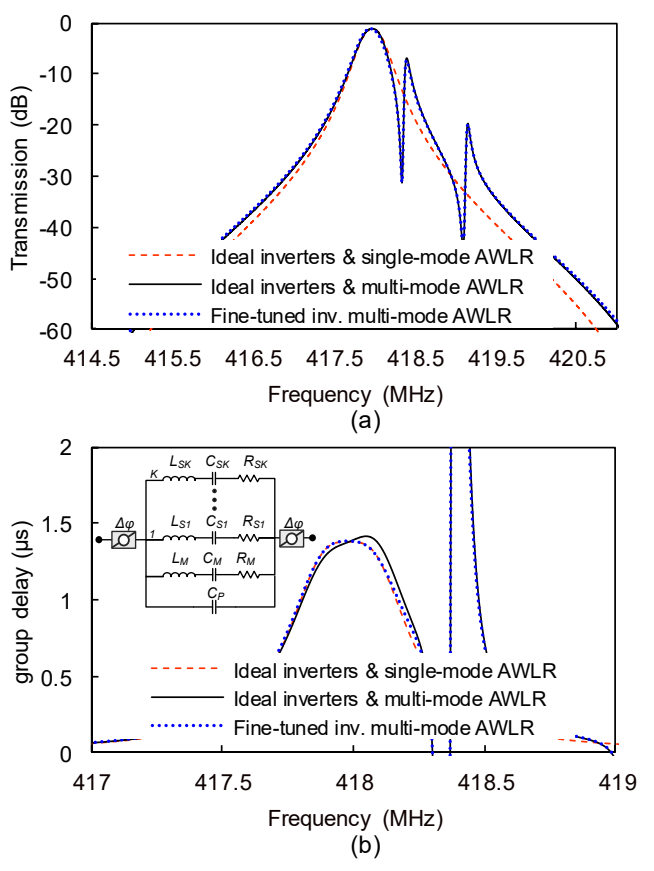


Fig. 8. Simulated power transmission response and τ_g of a two-pole/four-TZ AWLR-based BPF—Topology B—with constant in-band τ_g for acoustic-wave-resonators that comprise a single mode at ω_S (red trace) and two additional spurious modes (K=2) at the right-hand side of ω_S (black and blue trace). The impedance inverters are represented by 90°-long-at-418-MHz transmission lines with the following normalized impedance values. Red and black trace: $Z_{0,1}$ =1.92, $Z_{1,2}$ =1.95, $Z_{2,3}$ =1.02, and Z_{T} =2.8; blue trace: $Z_{0,1}$ =1.99, $Z_{1,2}$ =2.15, $Z_{2,3}$ =1.0, and Z_{T} =2.88. In addition, in the fine-tuned state the length of the $Z_{0,1}$ inverter is set equal to 99° at 418 MHz. Note that the single- and multi-mode acoustic-wave resonator circuit models correspond to the commercially-available ASR418S SAW resonator as discussed in [10].

The Q effect of the individual filter elements in the BPF transfer function is also shown in Fig. 7 for Topology B. It can be seen that the presence of finite Q in the inductor of the AWLR does not affect the in-band IL as also discussed in [10]. Thus, the extra loss that is observed in the BPF transfer function is due to the finite Q of the impedance inverters.

D. RF Design in the Presence of Spurious Modes

One of the fundamental limitations in acoustic-waveresonator-based filter design is the presence of spurious modes and, in particular, the ones located in a close proximity to their main resonance (ω_s). As discussed in [9]-[11], they can limit the maximum realizable BW for the main passband/stopband in bandpass and bandstop filter realizations, respectively. In this section, we investigate the effect of the spurious modes in the passband τ_g for a commercially-available acoustic-wave resonator (ASR418S from Abracon) with f_S =418 MHz, C_M = 1.21 fF, L_M =119.6 μ H, C_P =1.2 pF, and k_t^2 =0.08 %. Although Topology B is considered in this example, the same effects are expected for Topology A. Fig. 8 demonstrates example responses of a two-pole/four-TZ AWLR BPF that comprises AWLRs in which the acoustic-wave resonator is represented by its single-mode Butterworth-Van-Dyke model (red trace, K=0) and its extended multi-mode model (black trace, K=2) for two spurious modes, as described in [10]. It can be seen that the incorporation of the spurious modes results in in-band τ_g variation. This effect can be readily counteracted by finely tuning the impedance values of its corresponding impedance inverters as well as by adjusting the length of the $Z_{0,1}$ inverter from 90 to 99°—which allows to compensate the added phase shift $\Delta \varphi$ in the realistic multi-mode acoustic-wave resonator model, that is 4° in this case.

E. RF Diplexers with Constant In-Band Group Delay

The proposed AWLR-based concept can be further applied to the realization of RF diplexers as shown in the generalized block diagram in Fig. 9. The diplexer is shaped by two Nthorder AWLR-based BPFs based on the Topology A that are designed using the RF design methodology of Section II.A. They are connected at the common input port (node 1) through transmission lines that are appropriately designed in order to preserve the passband characteristics of each band in the presence of the other one. In the diplexer example in Fig. 9(a) and (b) they are set equal to the system reference impedance Z_0 and are 90°-long at the center frequency of each band—i,e., f2 for Z_{inv1} and f_1 for Z_{inv2} . As it can be seen, constant in-band τ_g can be obtained for both closely-spaced and widely-spaced bands. Furthermore, the illustrated response can be obtained by first selecting the impedance values using (1)-(3) and, if necessary, finely tune them as also discussed in Section II.A.

III. RF MEASUREMENTS AND DISCUSSION

In order to experimentally evaluate the RF design principles of the AWLR-based BPFs and diplexers with flat in-band τ_g , three different prototypes have been designed, manufactured, and measured using commercially-available one-port-type

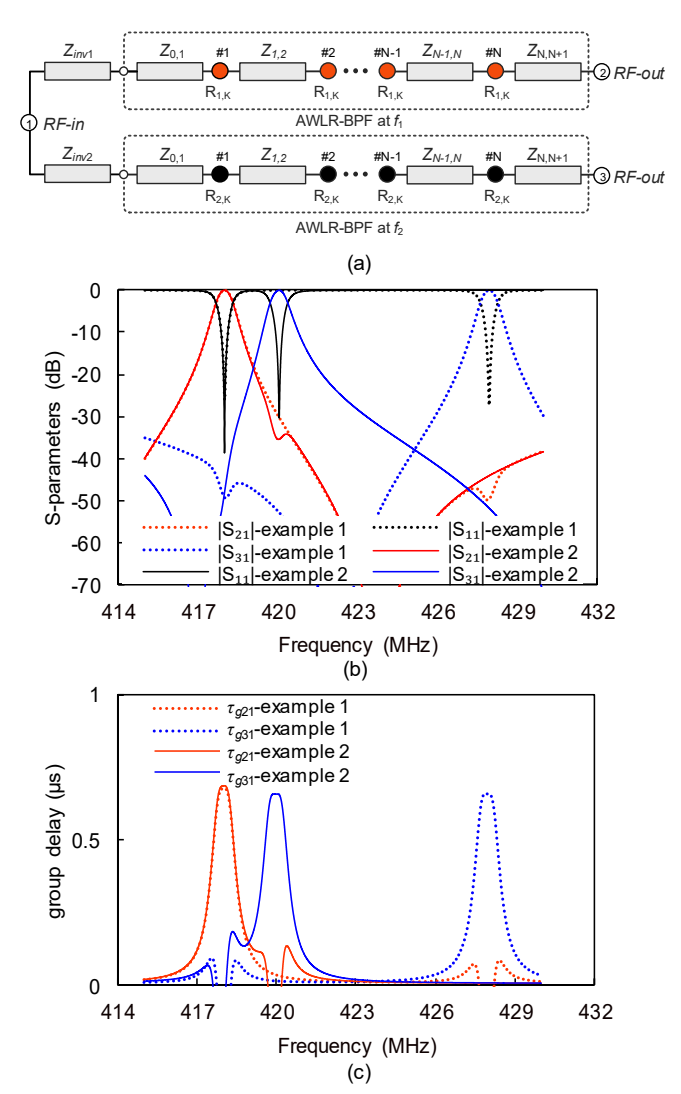


Fig. 9. Block diagram of an AWLR-based diplexer using AWLR BPFs based on the Topology A. (a) Block diagram. (b) Example S-parameter response for two channels each of them shaped by a two-pole/four-TZ AWLR BPF. (c) Example τ_g response for two-pole/four-TZ passbands. Example 1: widely-spaced bands; Example 2: closely-spaced bands.

SAW resonators (from Abracon and TDK EPCOS) and surfacemounted lumped elements (inductors: Coilcraft Inc.; capacitors: Johanson Tech.). They correspond to: i) a static three-pole/six-TZ AWLR BPF, ii) a tunable-BW twopole/four-TZ AWLR BPF, and iii) a diplexer with two passbands shaped by two poles and four TZs centered at 418 and 433.9 MHz respectively. The RF design of the aforementioned prototypes was performed using methodologies detailed in Section II. After defining the desired impedance inverter values, each of them was realized with its lumped-element circuit equivalent (first- or second-order, lowpass- or highpass-type). Post-layout full-EM simulations were performed using the Advanced Design System (ADS) software from Keysight Technologies in order to define the real filter layout (which also includes the landing pads for the SMD components and RF excitation) and its corresponding SMD components. A detailed description of each filter prototype along with EM simulated and RF measured results is provided below.

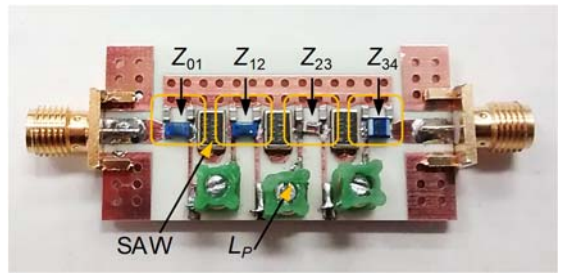


Fig. 10. Manufactured prototype of the three-pole/six-TZ AWLR BPF—Topology A—with constant in-band τ_g . All inverters were implemented with their first-order π -type circuit equivalent that comprises one series inductor from Coicraft inc. and two capacitors from Johanson Tech.. Z_{01} : C= 251R14S0R6AV4T and L= 12CS270, Z_{12} : C= 251R14S1R3BV4T and L= 10HQ47N, Z_{23} : C= 251R14S0R2AV4T and L= 10HQR10, and Z_{34} : C= 251R14S1R0BV4T and L= 10HQR56N.

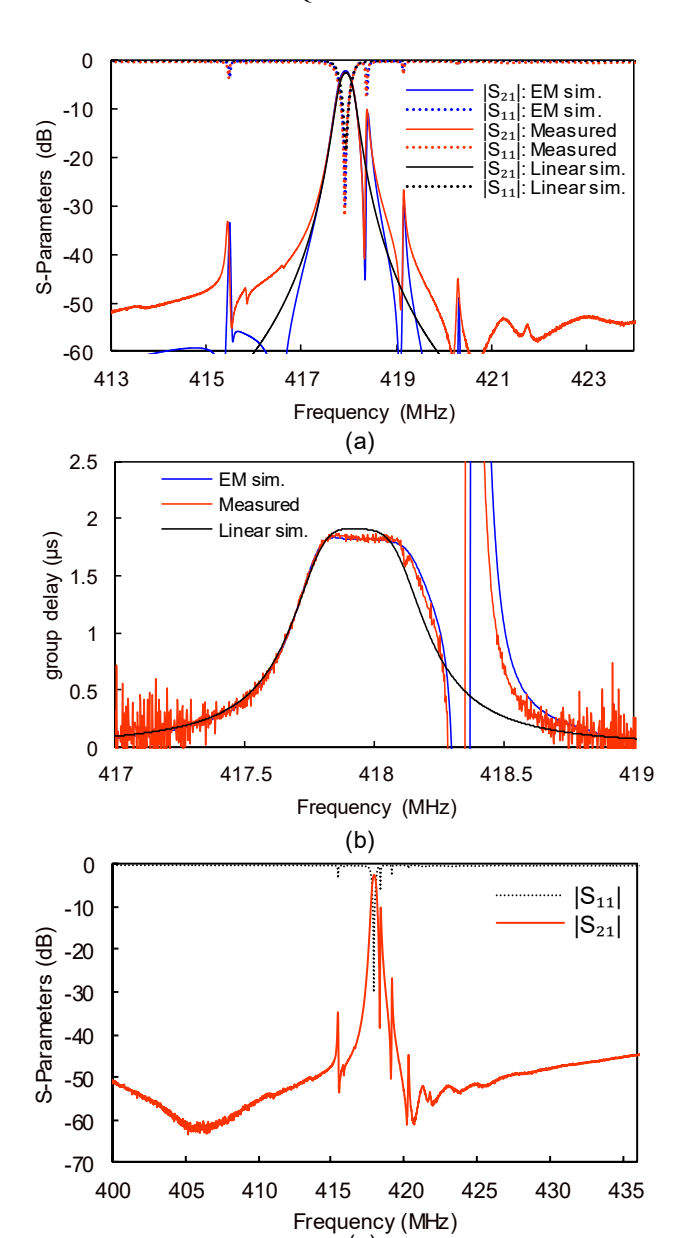


Fig. 11. Simulated (linear and EM using the multi-mode AWLR model) and RF-measured responses of the three-pole/six-TZ BPF prototype—Topology A—. (a) Power transmission and reflection responses. (b) τ_g . (c) RF measured response plotted in a broader frequency range.

A. Three-Pole/Six-TZ AWLR BPF with Flat In-Band Group Delay

The manufactured prototype of a three-pole/six-TZ AWLR-based BPF (Topology A) is illustrated in Fig. 10 along with its component values. It was built on a Rogers 4003 substrate with the following characteristics: dielectric permittivity ε_r =3.55, dielectric thickness H =1.52 mm, dielectric loss tangent $\tan(\delta_D)$ =0.0027, and 35 μ m-thick Cu-cladding. In addition, the SAW resonators are from Abracon and, in particular, the component ASR418S2 with C_M =1.211 fF, L_M =119.67 μ H, R_M =24.2 Ω , and C_P =1.59 pF has been employed.

The RF performance of the filter was evaluated in terms of S-parameters and τ_g through RF measurements and EM simulations which are shown in Fig. 11. In particular, Fig. 11(a) depicts its simulated and measured power transmission and reflection responses and Fig. 11(b) the τ_g . The RF measured response in a wider frequency range is shown in Fig. 11(c). The measured 3-dB BW, minimum in-band IL, return loss (RL), Q_{eff} , and in-band τ_g were extracted from the measured data in Fig. 10 and are respectively equal to 0.3 MHz, 2.1 dB, 32 dB, 9,000, and 1.78±0.02 us. Note that the measured passband exhibits a 2.4-times larger FBW $(0.95k_t^2)$ than in conventional ladder-type AWR-based BPFs as for example the ones in [3]-[8]. In addition, it exhibits a nearly-constant τ_g over the entire passband, which is much flatter than in acoustic-waveresonator-based BPFs in [13]-[16] for much lower minimum IL levels (2 dB instead of 5.2 to 25.5 dB) as summarized in the comparison table, Table I. It successfully demonstrates the merits of the proposed AWLR-based BPF with constant inband τ_g . The spurious resonances that are observed around the passband are due to the multi-resonant nature of the SAW element, as typically observed in all acoustic-wave resonatorbased-based BPFs [1]-[16]. A comparison between the RFmeasured, electromagnetically-simulated-AWLR modeled by its multi-mode circuit equivalent using the design methodology in [10]—, and ideally-synthesized (linear-circuit simulations) Sparameters and τ_g are also shown in Fig. 11. As can be seen, they are in a fairly-close agreement, successfully validating the practical viability of the devised filter concept.

B. Two-Pole/Four-TZ AWLR BPF with Tunable BW and Flat In-Band Group Delay

In order to evaluate the theoretical principles of the Topology

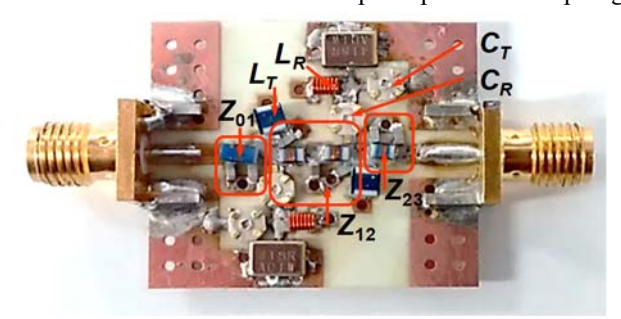


Fig. 12. Manufactured prototype of a tunable two-pole/four-TZ AWLR BPF—Topology B—. All inverters were implemented with their first-order π -type equivalent that comprises inductors from Coicraft inc. and capacitors from Johanson Tech.. Z_{01} : C= 251R14S4R3CV4T and L= 1206CS330, Z_{12} : C= 251R14S1R3BV4T and L= 0805HQ27N, and Z_{23} : C= 251R14S6R8CV4T and L= 0805HQ20N, L_T=1008HQ47N, C_T=C_R= Johanson 9701-1 (1-5 pF).

IABLEI
COMPARISON WITH STATE-OF-ART ACOUSTIC-WAVE-RESONATOR-BASED FILTERS

Design approach	$ au_g$	$ au_g$ variation	FBW	Loss	Estimated Q_{eff}	Out-of-band rejection	f_{cen}	Tuning	Ref.
	(ns)	(%)		(dB)		(dB)	(MHz)		
Conventional	38	±59.5#	$*0.6k_t^2$	1.3	2,300	>35	1592	No	%
Slanted transducers	695	±1.5	$^{*}0.6k_{t}^{2}$	25.5	<20	>70	70	No	[13]
Resonant transducers	563	± 6.7	$^{*}0.6k_{t}^{2}$	5.2	< 200	>40	140	No	[14]
Lossy elements	35	8.6	$*0.6k_t^2$	5.3	< 200	>28	1000	No	[15]
AWLR	1,780	±1.1	$>1k_{t}^{2}$	2.1	9,000	>45	418	Yes	This
									work

*Due to the lack of data on the filter topology, the FBW has been estimate around $0.6k_t^2$. Note that the FBW of acoustic-wave-resonator-based filters is between $0.4\ k_t^2$ and $0.8k_t^2$ based on [6]. #Estimated in the 3-dB-referred BW. f_{cen} denotes center frequency.
%Commercially-available SAW-based BPF: Abracon AFS14A35-1591.5-T3.

B concept, a two-pole/four-TZ filter prototype was built on a Rogers 4003 substrate with dielectric permittivity $\varepsilon_r = 3.55$, dielectric thickness H = 0.81 mm, dielectric loss tangent $\tan(\delta_D)$

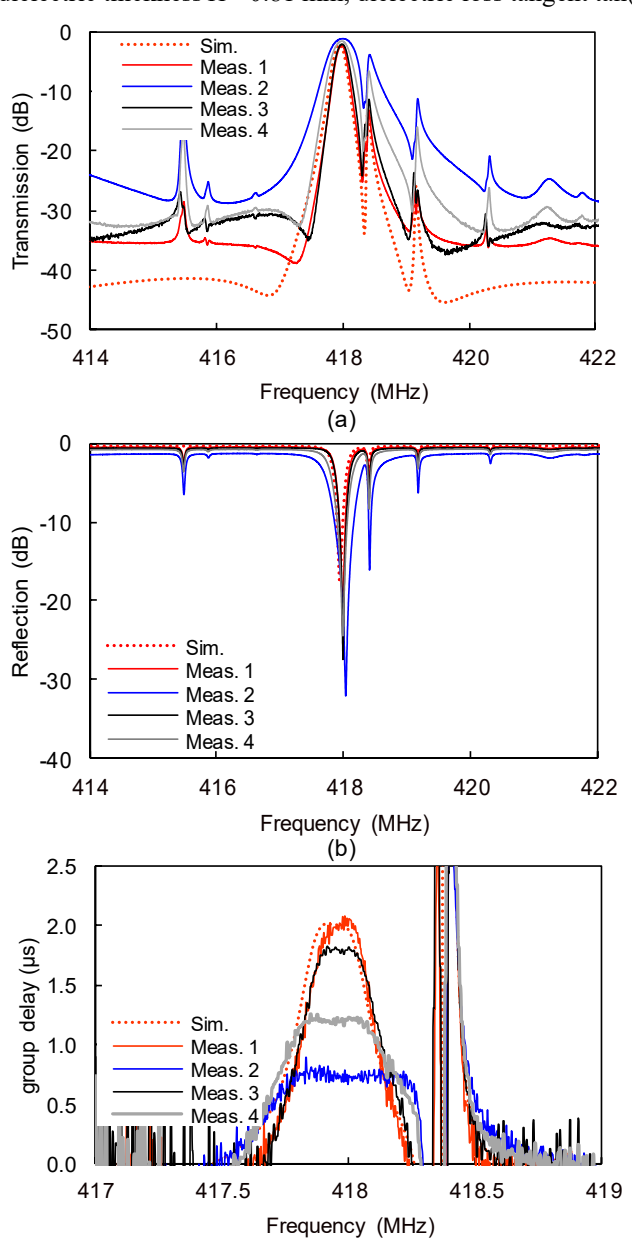


Fig. 13. RF-measured responses of the two-pole/four-TZ BPF prototype—Topology B— for various continuously-tunable BW states between 0.19 MHz and 0.45 MHz at 418 MHz. (a) Power transmission response. (b) Power reflection response. (c) τ_g .

(c)

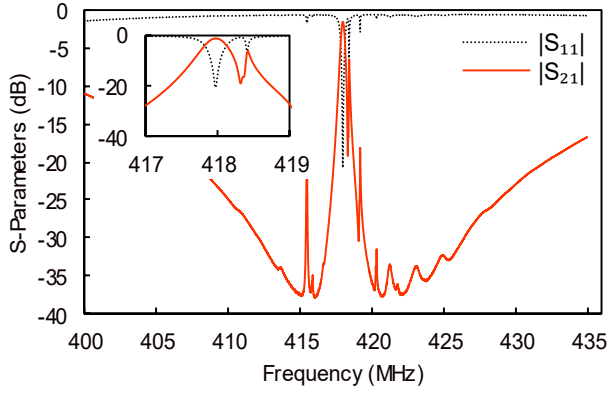


Fig. 14. RF-measured response for one reconfigure state of the two-pole/four-TZ BPF prototype—Topology B—in a broad frequency range and detail of its passband.

=0.0027, and 35 µm-thick Cu-cladding. The manufactured prototype along with its corresponding SMD elements are shown in Fig. 12. BW tunability was also implemented in this prototype by incorporating trimmer capacitors (1 pF to 5 pF) at the impedance inverters Z_T (C_T in Fig. 11) and at the AWLRs (C_R in Fig. 12). Fig. 13 demonstrates the BW-reconfiguration capabilities of the flat in-band τ_g AWLR BPF concept. As can be seen, analog BW tuning between 0.19 MHz and 0.45 MHz (i.e., 2.4:1 BW tuning ratio) can be obtained, which corresponds to a FBW tuning between $0.6kt^2$ and $1.4kt^2$. This successfully verifies the ability of this circuit for simultaneous FBW enhancement and analog-BW tunability with fairly constant inband τ_g for all tuning states. This is a unique advantage of the AWLR-based BPF concept in this work in relation to state-ofthe-art acoustic-wave-resonator-based filters, that are mostly static and exhibit large in-band τ_g variation. Furthermore, for the illustrated BW-tuning states in Fig. 13, the minimum inband IL was measured between 1.1 dB and 2.3 dB and the RL<18 dB, which correspond to an effective Q > 9,000 for all tuning states. Note that the SMA connector loss and RF excitation interface are included in the aforementioned IL values. A comparison between the EM-simulated response and one RF-measured state is also shown at the same figure. As can be seen, they are in a fairly close agreement to each other successfully validating the operating principles of the devised tunable-BW AWLR BPF with flat in-band τ_{σ} characteristics. Lastly, Fig. 14 shows the AWLR BPF response in a wider frequency range.

C. AWLR-Based Diplexer with Flat In-Band Group Delay The manufactured prototype of an example AWLR-based

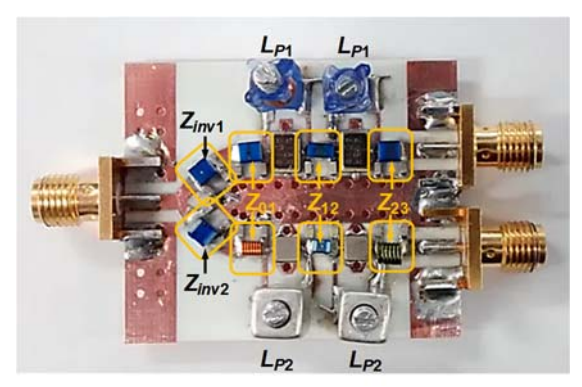


Fig. 15. Manufactured prototype of a diplexer that comprises two-pole/two-TZ AWLR BPFs—Topology B—. All inverters were implemented with their 1st-order π -type low-pass circuit equivalent that comprises one series inductor from Coicraft inc. and two capacitors from Johanson Tech. components for upper channel centered at 418 MHz: Z_{imv} !: C= 251R14S6R2CV4T and L= 1008CS180, Z_{01} : C= 251R14S5R6CV4T and L= 1008CS270, Z_{12} : C= 251R14S0R2AV4T and L= 1206CS560, Z_{23} : C= 251R14S1R3BV4T and L= 1008CS470, L_{P1}=165-06A06L, SAW= ASR418SR. Components for lower channel centered at 433.9 MHz: Z_{imv} !: C= 251R14S2R2CV4T and L= 0807SQ10N, Z_{01} : C= 251R14S6R8CV4T and L= 0806SQ19N, Z_{12} : C= 251R14S1R6AV4T and L= 0805CS430, Z_{23} : C= 251R14S1R8BV4T and L= 1111SQ39N, L_{P2}=164-04A06SL, SAW: EPCOS R900.

diplexer with flat in-band τ_g that comprises two channels, one located at 418 MHz and the other one at 433.9 MHz, is shown in Fig. 15. Although diplexers are typically designed for closely-spaced bands, in this example we have chosen the aforementioned frequencies based on the availability of commercial SAW resonators at the time that the design was performed. Each channel of the diplexer is shaped by a twopole/four-TZ AWLR BPF of Topology A and is designed using the guidelines in Section II.E. For the 418-MHz channel the Abracon ASR418S (f_S =418 MHz, C_M = 1.21 fF, L_M =119.67 μ H, R_M =24.2 Ω , and C_P =1.59 pF) SAW resonator was employed, whereas for the 433.9-MHz channel the EPCOS R900 (f_s =433.9 MHz, C_M = 1.62 fF, L_M =82.984 µH, R_M =19 Ω , C_P =1.97 pF) was used. Both filters are connected to the input junction through 90°-long transmission lines with characteristic impedance of 50 Ω as discussed in Section II.E. The filter components are shown in Fig. 15. Its measured response was evaluated in terms of Sparameters and τ_g that are depicted in Fig. 16. In particular, the 418-MHz passband exhibits the following characteristics: measured 3-dB BW of 0.27 MHz, minimum in-band IL of 2 dB, RL of 40 dB, $Q_{eff} > 7,000$, and in-band τ_g around 1.43 µs. The performances of the 433.9-MHz transmission band are as follows: measured 3-dB BW of 0.25 MHz, minimum in-band IL of 2.6 dB, RL of 13 dB, $Q_{eff} > 7,000$, and in-band τ_g around 1.65 µs. As can be seen, both bands feature fairly-constant inband τ_g that successfully validate the proposed design principle. Note also that despite the proposed concept has been verified for second-order channels, it can be readily extended to higherorder realizations or closely-spaced passbands.

D. Comparison with State-of-Art

Table I provides a comparison between the proposed AWLR BPF concept and alternative design techniques for flattening the in-band τ_g that can be found in the open technical literature. A comparison with a commercially-available SAW filter is also

shown. As mentioned in Section I, there is a limited number of approaches (only three) in which the design of flat in-band τ_g is addressed, namely the use of slanted transducers in [13], resonant transducers in [14], and the incorporation of lossy elements with dissimilar acoustic-wave resonators in [15] which results in significant amount of in-band IL despite the acoustic-wave resonators being high-Q. On the contrary, as an important advantage of the proposed approach, significantly-lower IL can be obtained with Q_{eff} of the order of 9,000 (Q_{eff} is < 200 in [13]-[15]) for the three-pole/six-TZ AWLR BPF prototype. In addition, the proposed design approach allows for enhanced FBW to be realized that is not limited by k_t^2 and can

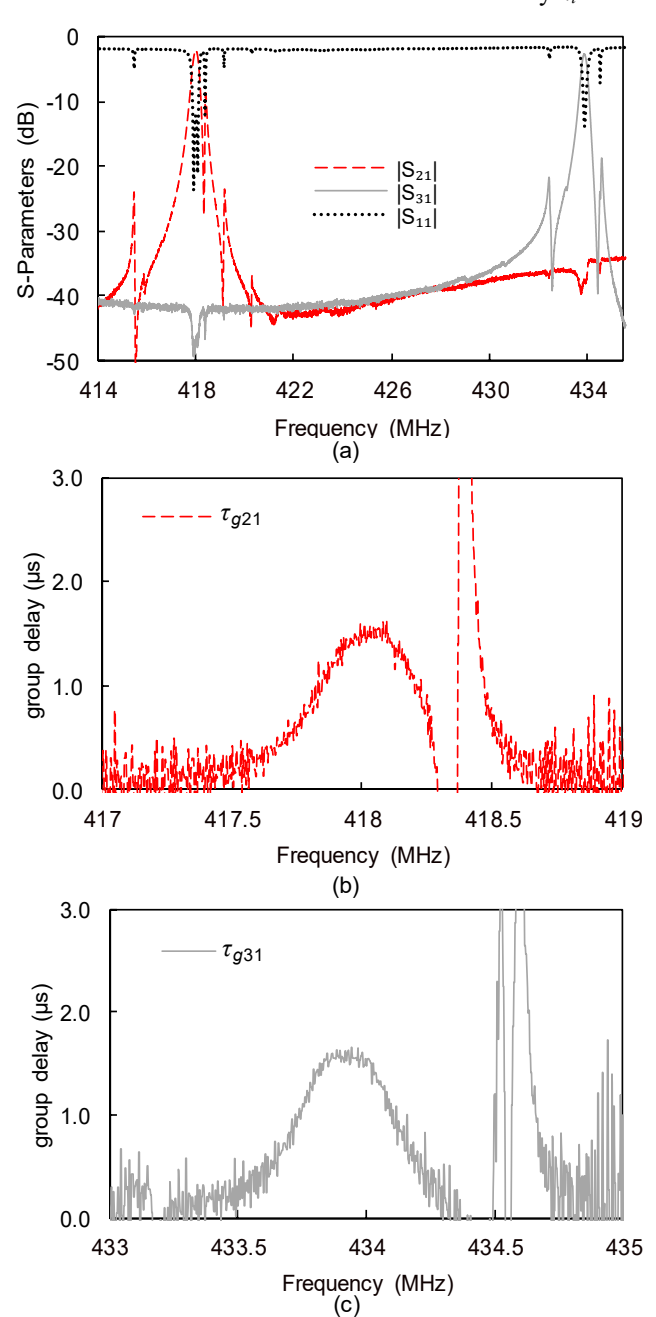


Fig. 16. RF-measured response of a diplexer shaped by two channels that comprise two-pole/four-TZ AWLR BPFs—Topology A—. (a) S-parameters. (b) Group delay of the lower channel (τ_{g21}). (b) Group delay of the upper channel (τ_{g31}).

be even made wider e.g., $1.4k_t^2$ for the two-pole/four-TZ AWLR BPF in this work. Lastly, as a unique advantage to be highlighted, the devised filter concept allows for analog-type BW tuning and up to 2.4:1 in this case whilst preserving the flat in-band τ_g characteristics for all tuning states. Note that all the filter topologies in Table I are static.

IV. CONCLUSION

This paper reported on a new class of AWLR-based BPFs with flat in-band τ_g and continuously-tunable BW. In relation to conventional acoustic-wave resonator-based BPF designs, the realization of constant in-band τ_g neither depends on k_t^2 nor requires lowering the Q of its constituent acoustic-wave resonators. In addition, the realized FBWs do not depend on k_t^2 and can be even made wider, which in turn results in enhanced FBW passbands. The operating principles of the AWLR BPF concept were evaluated through the following experimental prototypes: i) a static three-pole/six-TZ BPF ii) a tunable twopole/four-TZ BPF with 2.4:1 BW tuning range, and iii) a diplexer with two passbands centered at 418 MHz and 433.9 MHz respectively. They experimentally demonstrate the ability of this filter concept to functionalize quasi-elliptic-type transfer functions with simultaneous tunable BW and flat in-band τ_g using acoustic-wave resonators which is reported in this work for the first time.

REFERENCES

- [1] A. Link and P. Warder, "Golden age for filter design," *IEEE Microw. Mag.*, vol. 16, no. 7, pp. 60–72, Jul. 2015.
- [2] R. Aigner, "Filter technologies for converged RF-frontend architectures: SAW, BAW and beyond," in *IEEE Topical Meeting Silicon Monolithic Integr. Circuits in RF Syst. (SiRF)*, Jan. 2010, pp. 136–139.
- [3] R. Aigner, "SAW and BAW technologies for RF filter applications: A review of the relative strengths and weaknesses," in *IEEE Ultrason*. *Symp.*, Beijing, China, Nov. 2–5, 2008, pp. 582–589.
- [4] V. Lee, S. A. Sis, J. D. Phillips, and A. Mortazawi, "Intrinsically switchable ferroelectric contour mode resonators," *IEEE Trans. Microw. Theory Techn.*, vol. 61, no. 8, pp. 2806–2813, Aug. 2013.
- [5] M. Rinaldi, C. Zuniga, C. Zuo, and G. Piazza, "Super high frequency two-port AlN contour-mode resonators for RF applications", *IEEE Trans. Ultrason. Ferroelec. Freq. Control*, vol. 57, no. 1, pg. 38-45, 2010.
- [6] S. Gong and G. Piazza, "Multi-frequency wideband RF filters using high electromechanical coupling laterally vibrating lithium niobate MEMS resonators," in *IEEE 26th Int. MEMS Conf.*, Taipei, Taiwan, Jan. 20–24, 2013, pp. 785–788.
- [7] C. D. Nordquist, R. H. Olsson, S. M. Scott, D. W. Branch, T. Pluym, and V. Yarberry, "On/Off micro-electromechanical switching of AlN piezoelectric resonators," in *Proc. Microwave Symposium Digest*, 2013 IEEE MTT-S International, Seattle, WA, Jun. 2013, pp.1-4.
- [8] R. H. Olsson, J. Nguyen, T. Pluym, and V. M. Hietala, "A method for attenuating the spurious responses of aluminum nitride micromechanical filters," *J. Microelectromech. Syst.*, vol. 23, no. 5, pp. 1198–1207, Oct. 2014.
- [9] D. Psychogiou, R. Gómez-García, and D. Peroulis, "Coupling-matrix-based design of high-Q bandpass filters using acoustic-wave lumped-element resonator (AWLR) modules," *IEEE Trans. Microw. Theory Techn.*, vol. 63, no. 12, pp. 4319–4328, Dec. 2015.
- [10] D. Psychogiou, R. Gómez-García, R. Loeches-Sánchez, and D. Peroulis, "Hybrid acoustic-wave-lumped-element resonators (AWLRs) for high-Q bandpass filters with quasi-elliptic frequency response," *IEEE Trans. Microw. Theory Techn.*, vol. 63, no. 7, pp. 2233–2243, Jul. 2015.
- [11] D. Psychogiou, R. Gómez-García, and D. Peroulis, "High-Q bandstop filters exploiting acoustic-wave-lumped-element resonators (AWLRs)," *IEEE Trans. Circuits Syst. II, Exp. Briefs*, vol. 63, no. 1, pp. 79–83, Jan. 2016.

- [12] T. Komatsu, Y. Tanaka, K. Hashimoto, T. Omori and M. Yamaguchi, "Design of narrow bandwidth Ladder-type filters with sharp transition bands using mutually connected resonator elements", *IEEE Trans. Ultrason.*, *Ferroelect.*, *Freq. Contr.*, vol. 56, no. 7, pp. 1451-1456, Jul. 2007.
- [13] H.Yatsuda, "Design technique for nonlinear phase SAW filters using slanted finger interdigital transducers," *IEEE Trans. Ultrason., Ferroelec., Freq. Contr.*, vol. 45, no. 1 pp. 41–47, Jan. 1998.
- [14] H. Li, J. Wen, K. Hashimoto, T. Omori, and M. Yamaguchi, "Optimal design of an RSPUDT-based SAW filter with constant group delay," *IEEE Trans. Ultrason., Ferroelect., Freq. Contr.*, vol. 54, no. 10, pp. 1960 1964, Oct. 2007.
- [15] H. Wang, J. Chen, Y. Shi, T. Omori, C. Ahn and K. Hashimoto, "Design of Ladder-type SAW/BAW filters with constant group delay," in *IEEE Ultrason. Symp.*, Orlando, FL, USA, Oct. 18–21, 2011, pp. 345–348.
- [16] D. Psychogiou, R. Gómez-García, and D. Peroulis, "RF design of acoustic-wave-lumped-element-resonator-(AWLR)-based bandpass filters with constant in-band group delay," in *IEEE MTT-S Int. Microw. Symp. Digest (IMS)*, Honolulu, HI, USA, Jun. 4-9, 2017
- [17] J.-S. Hong, Microstrip Filters for RF/Microwave Applications, 2nd Ed., Hoboken, NJ, USA: Wiley, 2011.



Dimitra Psychogiou (S'10-M'14) received the Dipl.-Eng. degree in Electrical and Computer Engineering from the University of Patras, Patras, Greece, in 2008, and the Ph.D. degree in Electrical Engineering from the Swiss Federal Institute of Technology (ETH) Zürich, Switzerland, in 2013. From 2013 to 2016,

she was with Purdue University first as a Post-Doctoral Research Associate and then as a Senior Research Scientist. She is now an Assistant Professor of Electrical, Computer and Energy Engineering at the University of Colorado at Boulder, Boulder, USA. Her research focuses on RF design and characterization of reconfigurable microwave and millimeter-wave passive components, RF-MEMS, acoustic wave resonator based filters, tunable filter synthesis and frequency-agile antennas. Dr. Psychogiou has been serving as an Associate Editor for IET Microwaves, Antennas, and Propagation since 2015 and is a reviewer for several IEEE and IET, EuMA journals and conferences. Furthermore, she is an elected member of MTT-13 and URSI Commission D.



Roberto Gómez-García (S'02-M'06-SM'11) was born in Madrid, Spain, in 1977. He received the Telecommunication Engineer and Ph.D. degrees from the Polytechnic University of Madrid, Madrid, Spain, in 2001 and 2006, respectively. Since April 2006, he has been an Associate Professor with the Department of Signal Theory and

Communications, University of Alcalá, Alcalá de Henares, Madrid, Spain. He has been for several research stays in the C2S2 Department of the XLIM Research Institute (formerly IRCOM), University of Limoges, France, Telecommunications Institute of the University of Aveiro, Portugal, the U. S. Naval Research Laboratory (NRL), Microwave Technology Branch, Washington, DC, USA, and Purdue University, USA. His current research interests are in the design of fixed/tunable high-frequency filters and multiplexers in planar, hybrid and MMIC technologies, multi-function circuits and systems, and

software-defined radio and radar architectures for telecommunications, remote sensing and biomedical applications.

Dr. Gómez-García is the recipient of the 2016 IEEE MTT-S Outstanding Young Engineer Award and is an Adjunct Part-Time Professor at the University of Electronic Science and Technology of China, Chengdu, China. He was an Associate Editor of the IEEE Transactions on Microwave Theory and Techniques from 2012 to 2016, and the IEEE Transactions on Circuits and Systems-I: Regular Papers from 2012 to 2015. He was a Guest Editor of the IEEE Journal on Emerging and Selected Topics in Circuits and Systems 2013 Special Issue on "Advanced Circuits and Systems for CR/SDR Applications", the IET Microwaves, Antennas and Propagation 2013 Special Issue on "Advanced Tuneable/Reconfigurable and Multi-Function RF/Microwave Filtering Devices," and the IEEE Microwave Magazine 2014 Special Issue on "Recent Trends on RF/Microwave Tunable Filter Design". He is currently an Associate Editor of the IEEE Journal of Electromagnetics, RF and Microwaves in Medicine and Biology and the IET Microwaves, Antennas, and Propagation, and a Senior Editor of the IEEE Journal on Emerging and Selected Topics in Circuits and Systems. He is a reviewer for several IEEE, IET, EuMA, and Wiley journals. He serves as a member of the Technical Review Board for several IEEE and EuMA conferences. He is also a member of the "IEEE MTT-S Filters and Passive Components" (MTT-8), "IEEE MTT-S Biological Effect and Medical Applications of RF and Microwave" (MTT-10), "IEEE MTT-S Wireless Communications" (MTT-20), and "IEEE CAS-S Analog Signal Processing" (ASP) Technical Committees.



Dimitrios Peroulis (S'99–M'04–SM'15-F'17) received his PhD in Electrical Engineering from the University of Michigan at Ann Arbor in 2003. He has been with Purdue University since August 2003 where he is currently Professor of Electrical Engineering and the Deputy Director of the Birck Nanotechnology Center. His current research projects are

focused on the areas of reconfigurable electronics, RF MEMS, and sensors in harsh environment applications. He has been a key contributor on developing very high quality (O>1,000) RF MEMS tunable filters (1-100 GHz) in mobile form factors. Furthermore, he has been investigating failure modes of RF MEMS and MEMS sensors through the DARPA M/NEMS S&T Fundamentals Program, Phases I and II) and the Center for the Prediction of Reliability, Integrity and Survivability of Microsystems (PRISM) funded by the National Nuclear Security Administration. He received the National Science Foundation CAREER award in 2008. He has co-authored over 300 journal and conference papers. In 2014 he received the Outstanding Young Engineer Award of the IEEE Microwave Theory and Techniques Society (MTT-S). In 2012 he received the Outstanding Paper Award from the IEEE Ultrasonics, Ferroelectrics, and Frequency Control Society (Ferroelectrics section). His students have received numerous student paper awards and other student research-based scholarships. He is a Purdue University Faculty Scholar and has also received ten teaching awards including the 2010 HKN C. Holmes MacDonald Outstanding Teaching Award and the 2010 Charles B. Murphy award, which is Purdue University's highest undergraduate teaching honor.